Water harvesting using a conducting polymer: A study by molecular dynamics simulation

Mayur M. Ostwal, Muhammad Sahimi,* and Theodore T. Tsotsis
Mork Family Department of Chemical Engineering and Materials Science, University of Southern California, Los Angeles, California 90089-1211, USA

(Received 4 June 2008; revised manuscript received 24 February 2009; published 3 June 2009)

The results of extensive molecular simulations of adsorption and diffusion of water vapor in polyaniline, made conducting by doping it with HCl or HBr over a broad range of temperatures, are reported. The atomistic model of the polymers was generated using energy minimization, equilibrium molecular dynamics simulations, and two different force fields. The computed sorption isotherms are in excellent agreement with the experimental data. The computed activation energies for the diffusion of water molecules in the polymers also compare well with what has been reported in the literature. The results demonstrate the potential of conducting polyaniline for water harvesting from air.

DOI: 10.1103/PhysRevE.79.061801 PACS number(s): 82.35.Lr, 61.82.Pv, 81.07.De, 02.70.Ns

I. INTRODUCTION

Currently, the most important environmental issue is, perhaps, the global climate change that is being invoked to explain a wide variety of natural phenomena. The significance of climate change extends, however, beyond being the reason for some of the changes that are occurring in nature, as it also provides a new framework for recognizing the severity of a whole host of other problems, as well as their evaluation and granting them greater urgency. Such problems include, but not limited to, loss of biodiversity, desertification, and water scarcity. It is the last problem, and a method to address it, that is of interest to us in the present paper.

A recent report by the United Nations' Intergovernmental Panel on Climate Change [1] stated that there is water shortage for 1.1×10^9–3.2×10^9 people around the world. Such dire warnings have given rise to the research field of *water harvesting*—a field focused on developing new methods for harvesting water from sources that are freely, if not abundantly, available to us. They include rainwater and the water vapor in the atmosphere. While harvesting rainwater has been studied and used for a long time, absorbing the water vapor from the atmosphere and desorbing it in liquid form have been attracting attention only recently, despite the many advantages that such an idea has over those that are based on obtaining water from many other sources. Such advantages include the purity of the water, needing no filtration, purification, and sanitation. In addition, it is estimated that there are as much as 50 000 km^3 of water in the atmosphere at any given time, a great resource by any criterion.

Another important criterion for the efficiency of any method for water harvesting is the issue of distribution—the most difficult problem associated with water logistics and management. To better understand the problem, recall that conventional methods for water harvesting and purification, such as the reverse osmosis method, are adequate only if the water source and the communities to use it are close to each other. In most cases, however, the water resources are far from the utilization locations. It is precisely such cases for which water harvesting from air is extremely useful.

A few methods have already been suggested. For example, liquid desiccants have been proposed [2] for absorbing water. An example is hygroscopic salts, such as LiCl, with a free energy of hydration so large that, when exposed to typical ambient room air, it dissolves in its own water of hydration. Solid-state adsorbent has also been studied. A most important criterion for selecting any possible water absorbent or adsorbent is the amount of water that it can produce for every gram of the absorbing material.

We have recently been studying [3,4] the possibility of using a conducting polymer as a water adsorbent, by measuring the amount of water vapor that is absorbed by the polymer, when exposed to the air of a given relative humidity. Due to ionic solvation, such polymers absorb large amounts of water [5]. Moreover, their electrical [6–8] and chemical properties are modified [9–11] by the presence of water in their matrix, hence potentially creating other possible applications for such polymers. Sorption and transport of water vapor in conducting polymers are also of interest [5] due to the role of water or moisture content in the polymer's various other potential uses.

The particular conducting polymer that we have been studying for water harvesting from the air is polyaniline (PANI), a most promising material due to its straightforward preparation procedure and excellent chemical and mechanical stabilities. Other useful properties of PANI include its ease of processing into a low density high surface area-to-volume material, such as asymmetric and symmetric porous hollow fibers and flat sheets, solid nanofibers, textile fibers, and thin films. Electrical conduction in PANI and other conducting materials is due to their bonding structure along the backbone that consists of alternating single (s) and double (p) bonds. An electron may be added to the conjugated polymer backbone by a chemical reduction or *n*-type doping, or be removed from the polymer by chemical oxidation, or *p*-type doping. If the polymer's conjugation length is long enough, the charge travels freely down the conjugation paths, when an electrical potential is applied to the material. Depending on the extent of doping, the material's electrical conductivity varies anywhere [5,12] from semiconducting to metallic. The polymer's conductivity depends strongly on the

*Corresponding author; moe@iran.usc.edu

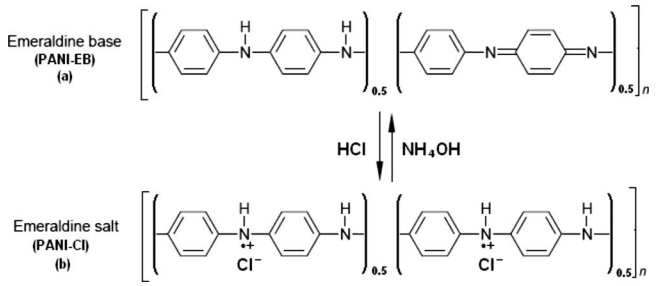

FIG. 1. The chemical structure of the emeraldine-base polyaniline (PANI-EB) and its doped version, i.e., emeraldine salt (PANI-ES).

type of the dopant, its structure and chemical heterogeneity, and the method by which it is processed and prepared. For example, anisotropic alignment of the polymer chains increases its conductivity by 2 orders of magnitude [13].

Although PANI has three oxidation states, only its emeraldine-base (EB) form, which is half oxidized and half reduced, can be chemically doped by a protonic acid to become conductive without changing its oxidation state. The polymer is also interesting because, unlike all other polymers in its class which require redox doping to become electrically conductive, any protonic acid can activate the PANI-EB, which consists of phenylenediamine and quinoid diimine units. Since there are two nitrogen atoms in the polymer's repeat unit, it is basic with $pK_a=8.6$. The acid/base chemistry or the doping process of PANI-EB is shown in Fig. 1 for doping it with a generic aqueous protonic acid (HX), as well as for the reverse reaction, known as dedoping, with a typical base, i.e., ammonium hydroxide. Upon doping, the electrically conductive form of PANI-EB is formed, which is known as the emeraldine salt. We point out that the dopant counterion is closely bound to the doped polymer's ionic unit sites by electrostatic forces, which serve to maintain the overall neutrality of the material. Hence, the volume conductivity of the polymer is truly electronic in nature, and not ionic.

In general, there are many other polymeric materials that absorb a significant amount of water. They do not, however, *desorb* the water molecules readily and, therefore, cannot be used for water harvesting from the humidity in the air. The electrical properties of doped PANI provide the basis for efficient coupling of the electrical energy with the adsorption/desorption of water, in such a way that the production of water is increased. More precisely, the water's adsorption free-energy minimum is less favorable when an electric current passes through the conducting PANI-EB. Thus, one may develop an efficient means of *desorbing* and producing large quantities of water, even under relatively dry conditions, by passing a small electric current through the PANI which has absorbed a considerable amount of water vapor from the air. Before the potential of the PANI for water harvesting can be fully transformed into reality; however, fundamental studies are needed in order to gain much deeper understanding of the phenomena involved.

However, despite the promise of the PANI as materials for efficient and cost-effective water harvesting through absorption of water vapor from the air, indicated by the experimental studies of its conducting form [3,4], many issues remain to be understood and resolved. The chief among such issues, as far as the practical applications of the concept are concerned, include the temperature dependence of the diffusivity of water vapor in PANI, as well as the effect of temperature on the adsorption isotherm and the amount of water vapor adsorbed. Such issues can be addressed only if there is fundamental understanding of how the structure and chemistry of a doped polymer, and in particular PANI, affect the transport and adsorption/desorption of water in the polymer.

In this paper we develop an atomistic model of doped PANI and utilize it to study diffusion and adsorption of water vapor in the polymer over a broad range of temperature that one may encounter in any potential large-scale application of water harvesting by the PANI. We study the PANIs that are doped with HCl (PANI-Cl) and HBr (PANI-Br). To validate the atomistic model, we compare the results of the molecular simulations with the experimental data. A few atomistic models of conducting polymers have already been developed [14–18]. None of them, however, studied the type of phenomena that we consider in this paper.

The rest of this paper is organized as follows. In the next section we describe the atomistic model of the conducting PANI that we have developed. We then describe in Sec. III the computation of the adsorption isotherms and the effective self-diffusivity of water in the PANIs, as well as the distributions of the cavity volumes in the doped and updoped polymers. The results are presented and discussed in Sec. IV, which also include the various pair-correlation functions that we have computed. The paper is summarized in Sec. V, where we also discuss some future directions in this area of research.

II. ATOMISTIC MODELS

We have utilized two atomistic models of the PANI, as well as a well-established molecular model of water, in order to carry out the molecular simulations and study the effect of the atomistic models on the results. In what follows we describe the models and explain the simulation procedure.

A. Models of the polymer

A modified version of the self-avoiding walk (SAW) method of Theodorou and Suter [19] was used to generate the initial structure of the PANI. Their rotational isomeric state method was intended mainly for vinyl polymer glasses. In order to utilize the method for generating the structure of the PANI, we modified [20] the method in order to better represent the polymer. A cubic simulation cell was used in which three atoms of the PANI's backbone that are connected by bonds were placed in random orientations. The polymer structure was then constructed by adding one atom at a time in a stepwise fashion, using the modified SAW algorithm [19,20]. The allowed rotational states of the successive bonds between adjacent atoms were determined from the probability distribution functions that were governed by energy considerations (see below). To suppress the surface effects, periodic boundary conditions were used.

Two different force fields were utilized in order to generate the atomistic model of the PANI. The two force fields

TABLE I. Values of the force constants K_i and the equilibrium lengths l_0 for various pairs. H and N are hydrogen bonded.

Pair	l_0 (Å)	K_2	K_3	K_4
C-C	1.417	470.836	−627.618	1327.635
C-H	1.0982	372.825	−803.453	894.317
C-N	1.391	447.044	−784.535*a*	886.167
H-N	1.002	465.861	−1066.236	1496.565
H-O	0.97	563.28	−1428.22	1902.12

also made it possible to study the effect of the atomistic details of the polymer model on the results presented below. One force field that we utilized was the polymer-consistent (PC) force field in which the total potential energy E of the polymer is given by

$$E = E_s + E_\theta + E_\phi + E_{\rm nb}, \tag{1}$$

with

$$E_s = \sum_{i=2}^{4} K_i (l - l_0)^i, \tag{2}$$

$$E_\theta = \sum_{i=2}^{4} H_i (\theta - \theta_0)^i, \tag{3}$$

$$E_\phi = \sum_{i=1}^{3} D_i (1 - \cos i\phi), \tag{4}$$

$$E_{\rm nb} = \sum_{i,j} \frac{q_i q_j}{r_{ij}} + \sum_{ij} \varepsilon_{ij} \left[2\left(\frac{\sigma_{ij}}{r_{ij}}\right)^9 - 3\left(\frac{\sigma_{ij}}{r_{ij}}\right)^6 \right], \tag{5}$$

where

$$\sigma_{ij} = \left[\frac{1}{2}(\sigma_i^6 + \sigma_j^6) \right]^{1/6}, \tag{6}$$

$$\varepsilon_{ij} = 2\sqrt{\varepsilon_i \varepsilon_j} \frac{\sigma_i^3 \sigma_j^3}{\sigma_i^6 + \sigma_j^6}. \tag{7}$$

E_s is the energy associated with bond stretching, where l_0 is a bond's equilibrium length, l is its actual length at any time during the simulations, and K_i is a stretching-force constant. Values of K_i and the equilibrium lengths l_0 are listed in Table I for all the pairs. E_θ represents the energy associated with the changes in the bonds' angles, where θ_0 is the equilibrium angle of a bond, θ is its angle at any given time during the simulations, and H_i is the corresponding force constant. Numerical values of H_i and θ_0 are listed in Table II for all the triplets. The contribution of the torsional forces is represented by E_ϕ, with D_i being a force constant and ϕ being the dihedral angle. Values of the parameters are given in Table III for all the quadruplets. $E_{\rm nb}$ represents the contributions to the total energy E of the nonbonded interactions due to the Coulombic and the van der Waals interactions, with the latter represented by a 6-9 Lennard-Jones (LJ) potential. In Eq. (5)

TABLE II. Values of the force constants H_i and the equilibrium angle θ_0 for various triplets. H and N are hydrogen bonded.

Triplet	θ_0 (deg)	H_2	H_3	H_4
C-C-C	118.90	61.023	−34.993	0
C-N-H	111.87	40.837	−15.667	0
C-C-H	117.94	35.156	−12.468	0
C-C-N	121.46	61.064	−21.616	0

σ_i and ε_i are the LJ size and energy parameters for atom i, r_{ij} is the distance between (the centers of) atoms i and j, and q_i is the *partial* charge of i. The nonbonded interactions were cut off at an interatomic distance of 12.5 Å, while a spline switching function was used between 9.5 and 12.5 Å. The cutoffs were selected carefully, based on extensive preliminary simulations, as well as our previous extensive experience with modeling of Coulombic interactions using the multipole expansion [21] and the Ewald summation [22] techniques. (Other methods of simulating Coulombic interactions are also available [23].) Perhaps it would have been somewhat more accurate to also include some corrections due to the introduction of the cutoffs; but for the main purpose of the present work, namely, testing the accuracy of the atomistic models of the doped PANI for providing reasonably accurate predictions of the sorption isotherms and the diffusivities, the cutoffs without any corrections seem to suffice (see below). Values of the parameters used in the nonbonded part of the PC force field are listed in Table IV. Most of the results presented in this paper were obtained using the PC force field.

Note that while the *formal charges* of Cl and Br are −1, their *partial charges* q_i take on very small negative values, as listed in Table IV. Note also that, with the partial charges that are listed in Table IV, the doped polymer is electrically neutral. Consider, for example, the PANI-Cl. The atomistic model that we construct for the doped polymer contains 481 C of the C-H type, 239 C of the C-N type, 481 H of the H-C type, 121 H of the H-N type, 119 N atoms, and a single truncated nitrogen atom, denoted by N^* in Table IV. Recall that one nitrogen atom is shared by two carbon and one hydrogen atoms. N^* is called the truncated atom because the polymer is constructed by attaching the monomers (N) to the tail atom. Therefore, with such numbers of the atoms, the PANI-Cl that we construct is electrically neutral, and simi-

TABLE III. Values of the force constants D_i for various quadruplets. H and N are hydrogen bonded.

Quadruplet	D_1	D_2	D_3
C-C-C-C	8.367	1.193	0
C-C-C-H	0	3.966	0
C-C-C-N	0	5.383	0
H-C-C-H	0	1.877	0
H-C-C-N	0	1.333	0
C-C-N-H	0	1.219	0

TABLE IV. Values of the parameters for the nonbonded part of the PC force field. H and N are hydrogen bonded. N^* is the truncated nitrogen atom, since the polymer is constructed by attaching the monomers, i.e., N^*, to the tail atom.

Atom	Type	σ_i (Å)	ε_i (kcal/mol)	q_i (electron)
O	H_2O	3.608	0.274	−0.798
H	H_2O	1.098	0.013	0.399
C	C-H	4.010	0.064	−0.1268
C	C-N	4.010	0.064	0.0827
H	C-H	2.995	0.020	0.1268
H	N-H	1.098	0.013	0.2499
N		4.070	0.065	−0.4141
N^*		4.070	0.065	−0.5801
Br		4.215	0.305	−0.01
Cl		3.915	0.305	−0.01

larly for the PANI-Br. It is also easily seen that the water molecules are neutral.

Less extensive simulations of the adsorption of water vapor in the doped polymers were carried out with a second force field, namely, the *ab initio* optimized COMPASS force field [24] of the CERIUS^2 package from Accelyrs [25]. In the COMPASS force field the bonded terms are derived from the Hartree-Fock calculations [26], while the nonbonded terms of the force field are similar to Eq. (5) (but with, of course, a different set of parameters). The COMPASS force field has recently been used for modeling the PANI [27].

The initial polymer was then doped with HCl. A polymer doped by HBr was also generated. The doping process was simulated by the following method. First, a repeating unit of the PANI-EB was constructed [see Fig. 1(a)]. We then broke the double bonds between nitrogen and carbon atoms in the diimine units, and hydrogen and Cl, or Br, atoms were attached to the nitrogen atoms through single bonds in alternating positions [see Fig. 1(b)]. The polymer was then constructed using 30 repeating units [see Fig. 1(b)], after which all the bonds between the nitrogen and the Cl, or Br, atoms were broken. This procedure generated doped PANI-Cl or PANI-Br. Sixty Cl or Br atoms, equivalent to 1.0 mol of HCl or HBr, were added to the polymer and, therefore, the polymer was fully doped.

B. Model of water

Due to its relatively complex structure, the precise model of the water molecules may have a significant effect on the results. Various models of water have been developed in the past [28]. What we utilized was the well-known simple point charge-extended (SPC) model [29] which was also utilized in our previous work [22] on hydration properties of hydrotalcites. The two hydrogen and the oxygen atoms are all represented by the LJ spheres, with the size and parameters listed in Table IV. The H-O-H angle was held fixed at 109.5°. Partial charges were also assigned to the hydrogen and oxygen atoms, the values of which are listed in Table IV. The sphere with the oxygen atom located at its center corresponds to the site responsible for the dispersive oxygen-oxygen interactions, described by a LJ potential. The sites that represented the H atoms were fixed at a distance of 0.97 Å from the O site.

The SPC model of water was used in the past to simulate the adsorption of water in porous carbon and carbon nanotubes [30], and on calcite [31]. Others have used simple LJ-type models of water (representing it by a *single* LJ sphere) to simulate its adsorption on activated carbons [32] and in silicalite membranes [33]. Rahaman *et al.* [34] used a more sophisticated model of water—the POL3 model of Caldwell and Kollman [35]—to study adsorption of water on a calcite surface. In the POL3 model the energy of the system contains quadratic terms for the stretching and angle-changing contributions, while the torsional and nonbonded terms are similar to Eqs. (4) and (5), respectively, except that the parameters are determined by quantum-mechanical computations, rather than by fitting them to experimental data.

C. Generation of the model of the doped polymer

Energy minimization and molecular dynamics (MD) simulations were utilized in order to generate the atomistic model of the doped PANI. The density of the polymer at the beginning of the energy minimization was set to be 0.15 g/cm^3, so as to avoid ring spearings and catenations. The total energy E of the polymer was then minimized using the conjugate-gradient method [36]. To increase the density, the simulation box was compressed at pressures between 0.5 and 0.9 GPa, and the MD simulations were carried out in the (NPT) ensemble for several nanoseconds. The total energy of the resulting polymer was again minimized. To obtain the structure at equilibrium, MD simulations were carried out in the (NVT) ensemble at 1000 K, after which the system was gradually cooled down, using steps of 50–325 K.

We then carried out MD simulations in the (NPT) ensemble for several ns at 1 atm and 325 K. The time step used was 1 fs. The pressure was controlled by the Andersen method [37], while the temperature was held fixed using the Nosé-Hoover thermostat [38]. For the Andersen barostat the masslike parameter W is equal to the cell-mass prefactor times the total mass of the atoms in a unit cell. We used $W=20.0$ amu. For the Nosé-Hoover thermostat one must specify the value of the quantity which is used to scale the fictitious mass in the thermostat; we used a value of 1.

Figure 2 presents the change with the time of the energy of the PANI-Cl at two temperatures. It is clear that the energy of the material has reached its true minimum at both temperatures. Similar results were obtained for the PANI-Br, samples of which are shown in Fig. 3. As both figures indicate, we ensured that each MD run was long enough for obtaining representative values of the energy at equilibrium. We note, however, that while the constancy of the total energy of the polymer may be a good indication of whether the polymer has attained its true equilibrium configuration, it might not be sufficient under certain conditions and, therefore, other properties of the polymer must also be studied. For example, one may check the longest chain dimension,

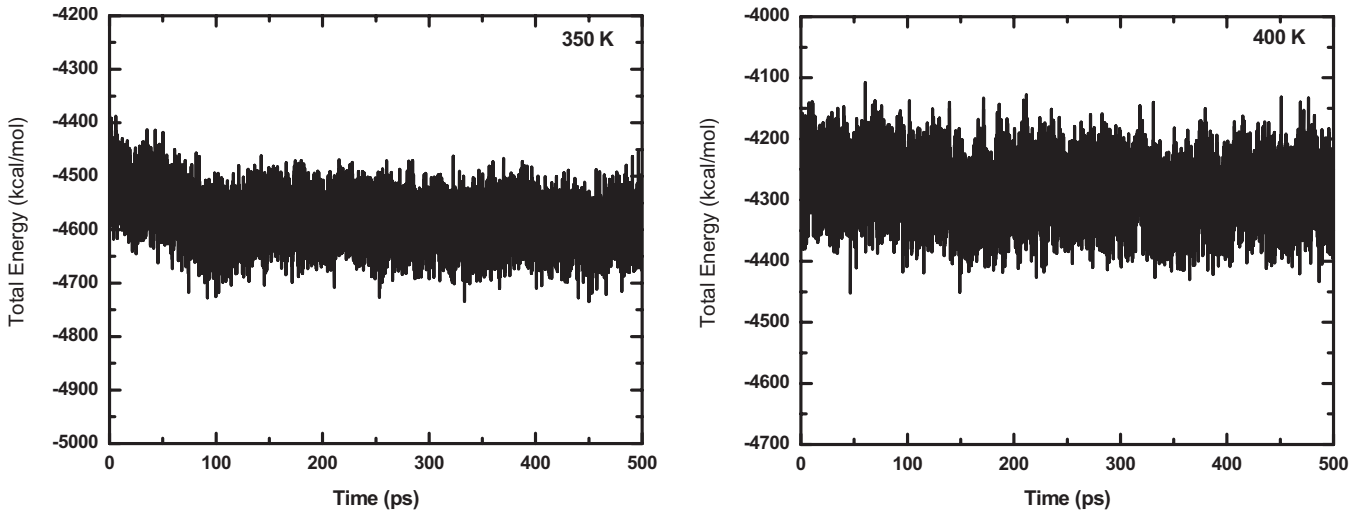

FIG. 2. Time dependence of the energy of the PANI-Cl during energy minimization and MD simulations.

i.e., the chain's end-to-end distance, and the longest characteristic time that can be computed by calculating the rotational relaxation time. There are also other efficient methods of achieving accurate equilibration of a polymer's structure [39].

The same procedure was also used for generating the doped polymers at all the temperatures. The final (equilibrium) densities of the polymers so obtained are shown in Fig. 4, where the measured densities of PANI-Cl and PANI-Br (1.3 g/cm^3) at 298 K are also given. Figure 5 presents samples of the doped polymers at the end of the simulations.

III. SIMULATION OF ADSORPTION AND DIFFUSION OF WATER VAPOR

To assess how much water vapor can be absorbed by the doped PANI, and how fast the water molecules move in the polymer, we carried out MD simulations of adsorption and diffusion of water molecules in the polymer. The rate of transport in a polymer, and in particular the effective diffusivity, depends to a large extent on the cavity or free-volume distribution of the polymer. This is particularly important for a doped polymer, as one would like to understand how the doping may affect the cavity size distribution. Thus, we also computed the cavity size distribution of the doped and undoped PANIs. In what follows we describe the simulations.

A. Simulation of adsorption

Two methods were used for computing the adsorption isotherms of water vapor in the doped PANIs. One was the particle-insertion method of Widom [40], which is just a way of computing the chemical potentials, when a number of adsorbate molecules are added to the system. Thus, we first added ten H_2O molecules to the simulation cell that contained the PANI-Cl or the PANI-Br. The total energy of the system was then minimized. Subsequently, the polymer structure in the presence of the water molecules was equilibrated with the aforementioned procedure, followed by MD simulation in the (*NVT*) ensemble for 2 ns at a given temperature *T*. After each MD simulation with a duration of 50

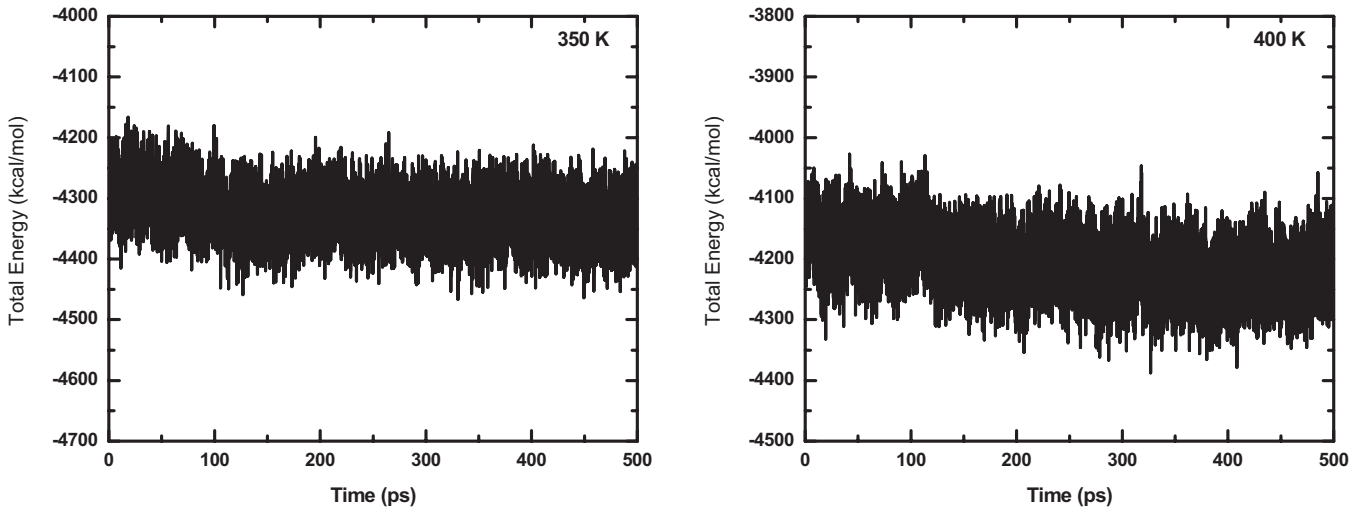

FIG. 3. Same as in Fig. 2, but for the PANI-Br.

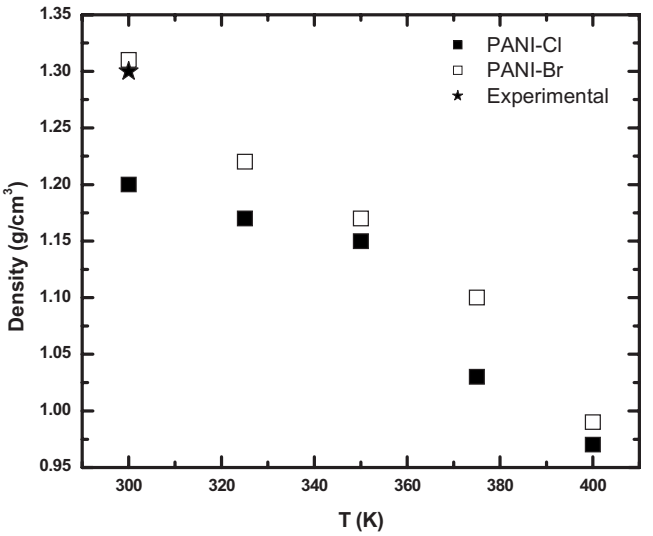

FIG. 4. Temperature-dependence of the density of the PANI-Cl and PANI-Br polymers.

ps, a polymer configuration was extracted, for a total of 40 configurations for the entire simulation. The configurations were then used in the particle (ghost H_2O molecule)-insertion simulation. Because the chemical potential of the polymer without the water is the same as that of the bulk, the *excess* chemical potential of the system—the polymer+the water molecules—was then computed using

$$\mu_e = -k_B T \ln\langle \exp(-\Delta E/k_B T)\rangle, \tag{8}$$

where k_B is the Boltzmann constant, ΔE is the change in the energy of the material as a result of adding the water molecules to it, and $\langle \cdot \rangle$ denotes an ensemble average over all the configurations. To obtain reliable statistics, up to 2×10^5 particle insertions were attempted for each configuration, in order to compute ΔE and, hence, μ_e. Typically, a few percents of the insertions were successful, which provided reliable statistics, due to the large number of the insertion trials. Next, 20 more water molecules were added to the system (that already contained the first 30 H_2O molecules) and the above procedure was repeated, in order to compute μ_e. The same procedure was repeated with several larger numbers of water molecules in the system, and at several temperatures (see below).

We also utilized the grand-canonical Monte Carlo (GCMC) technique to compute the sorption isotherms. The GCMC method, which represents simulations in a (μTV) ensemble, has also been used extensively for computing the sorption isotherms in nanopores and nanoporous materials. A chemical potential μ is set, and the water molecules are inserted in the system with their probability of acceptance being,

$$p^+ = \min\left\{\frac{ZV}{N+1}\exp(-\Delta E/k_B T), 1\right\}, \tag{9}$$

where Z is the absolute activity at temperature T, ΔE is the potential energy change resulting from inserting (or removing) a water molecules, and V and N are the volume of the system and the number of the atoms, respectively. The probability of removing a water molecule from the system is given by

$$p^- = \min\left\{\frac{N}{ZV}\exp(-\Delta E/k_B T), 1\right\}. \tag{10}$$

After a few insertions or deletions the system is again allowed to equilibrate since the polymer responds to the presence of the water molecules. The procedure is repeated until the desired chemical potential is reached, at which time the number of accepted water molecules is recorded. The chemical potential is then increased (or decreased) to another value, and the procedure is repeated.

We note that it is important to allow a sufficient number of equilibration steps to bring the system to true equilibrium with the reservoir of the fluid at the new fugacity. The first simulation in the specified fugacity range starts from an empty sorbent system. Subsequent simulations start from the final configuration of the previous simulation. The required

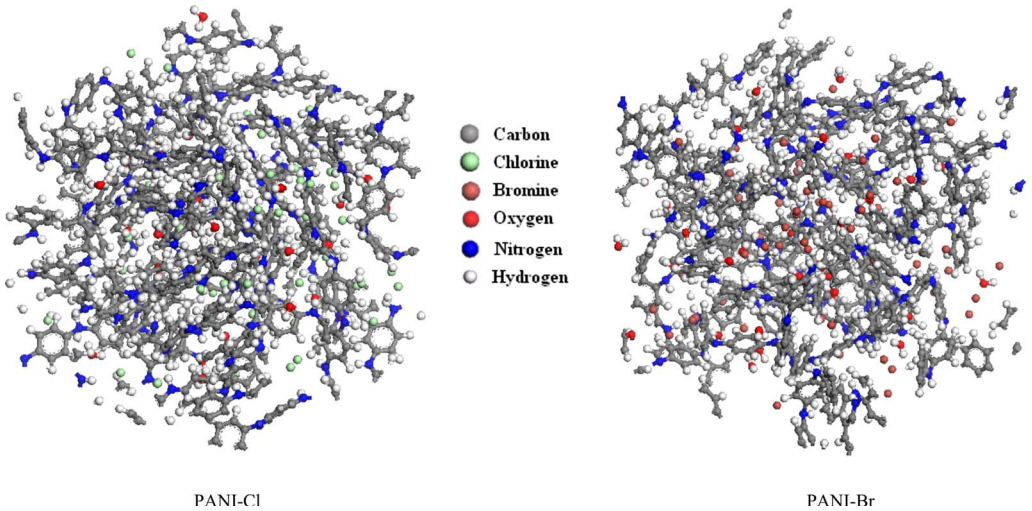

FIG. 5. (Color online) The structures of the doped polymers, obtained by energy minimization and MD simulations, at 350 K.

number of equilibration steps generally increases with fugacity. Thus, care was taken to ensure that such requirements were met during the simulations.

Because the sorption isotherms are usually represented in terms of the pressure, the computed μ_e (in the particle-insertion method) or the specified chemical potentials (in the GCMC method) were converted to pressure using the LJ equation of state, given by Johnson *et al.* [41]. This, of course, provides only approximate estimates of the pressure but, as shown below, it still led to good agreement with the experimental data for the sorption isotherms.

B. Self-diffusivity

The self-diffusivities D of water vapor in the PANI-Cl and PANI-Br were estimated using the random-walk method. For a given temperature, we first added 30 water molecules to the simulation cell that contained the doped polymer. The energy of the system was then minimized, followed by its compression and equilibration/relaxation using the above methodology. We then carried out MD simulations in the (NVT) ensemble with the duration that, depending on the temperature, was 4.2–7 ns. The self-diffusivity was then computed from the mean-square displacements (MSDs) of the water molecules using

$$D = \lim_{t\to\infty} \frac{1}{6t} \langle |R(t) - R(0)|^2 \rangle, \tag{11}$$

where $\langle \cdot \rangle$ represents an average over all the water molecules and $R(t)$ is the position vector of a water molecule at time t. The MSDs were also averaged over all the possible origins of the H_2O molecules in the system.

C. Distribution of the accessible free volumes

To compute the cavity or free-volume distributions of the doped and undoped PANIs, MD simulations in the (NPT) ensemble were carried out in the absence of the water molecules. Twenty configurations, taken every 100 fs, were extracted for each of the three polymers (PANI-Cl, PANI-Br, and undoped PANI) from the simulation trajectories. The accessible free volumes of the polymers were then computed using the following method based on a hard-sphere probe.

(i) The cubic simulation cell was partitioned into a three-dimensional mesh of $100 \times 100 \times 100$ subcells.

(ii) A probe molecule—a hard sphere—of a given diameter was inserted at the center of each subcell, and the distance to the nearest atom of the material was computed. If the distance turned out to be larger than the sum of the van der Waals radii of the penetrant molecule and the material's atom, the subcell was considered as contributing to the accessible free volume. The cavity size distributions of the polymers were then computed using a Voronoi tessellation of the space, based on the algorithm of Tanemura *et al.* [42]. The vectors connecting (the centers of) the atoms in the system were perpendicularly bisected and a large number of intersecting planes were generated. The polyhedra associated with the atoms were then constructed using the algorithm. As a Voronoi polyhedron around an atom identifies its own available space, it can be related to the void volume of the polymer, which was then used to study the distribution of the free volumes.

IV. RESULTS AND DISCUSSION

The computed results are divided into four groups. In one group are those that characterize the structural properties of the doped PANIs and how the water molecules interact with them. Sorption and diffusion results are in the second and third groups, respectively. In the last group are the activation energies for the diffusion process. In what follows we present and discuss the results.

A. Structural properties

Figure 4 presents the temperature dependence of the densities of PANI-Cl and PANI-Br. The computed densities of PANI-Cl and PANI-BR at 298 K are, respectively, about 1.20 and 1.32 g/cm^3, both of which are reasonably close to the experimental density of 1.3 g/cm^3. We are not aware of any experimental data for the densities at any other temperature. Both densities decrease with increasing temperature, but do not follow similar trends.

Depending on the temperature, the simulation cell's length varied from 26 to about 29 Å. The structures of the simulated PANI-Cl and PANI-Br at 350 K are shown in Fig. 5, along with the inserted water molecules. There are visible differences between the structures of the two doped polymers that are due to the presence of Cl and Br anions. Such differences also affect the sorption isotherms and the self-diffusivities of water vapor in the two polymers, which will be described below.

Figure 6 compares the distributions of the cavity volumes v of the PANI-Cl at three temperatures. They appear to be bimodal. The small cavities are relatively abundant and narrowly distributed in the range $5 \leq v \leq 12$ $Å^3$, with a maximum at about 8 $Å^3$. Larger cavities have volumes of up to 40 $Å^3$. As T increases, a small but significant fraction of cavities appear with volumes $v > 40$ $Å^3$. In fact, at 400 K there are cavities that have volumes of up to 60 $Å^3$. At the same time, the relative frequency of the smaller cavities decreases by about 15%. Qualitatively similar trends are seen for the cavity volume distribution of the PANI-Br, except that the smaller cavities have lower frequencies than those in the PANI-Cl, while larger cavities form more frequently. This is shown in Fig. 7.

To understand the effect of doping of the PANIs on their cavity distribution, we present in Fig. 8 a comparison between the cavity volume distribution of the undoped PANI with those of the PANI-Cl and the PANI-Br at 298 K. When doped by Br, the resulting polymer, PANI-Br, acquires a few large cavities, as a result of which the tail of the cavity volume distribution is longer than that of the PANI-Cl distribution. At the same time, the PANI-Cl has a larger number of smaller cavities, indicated by the two more pronounced maxima in its cavity distribution. The cavity volume distribution of the undoped PANI, on the other hand, has a relatively short tail with very few large cavities, which vanishes beyond 27 $Å^3$. Such differences affect the adsorption isotherms and the diffusivity of water molecules in the three materials, which will be described shortly.

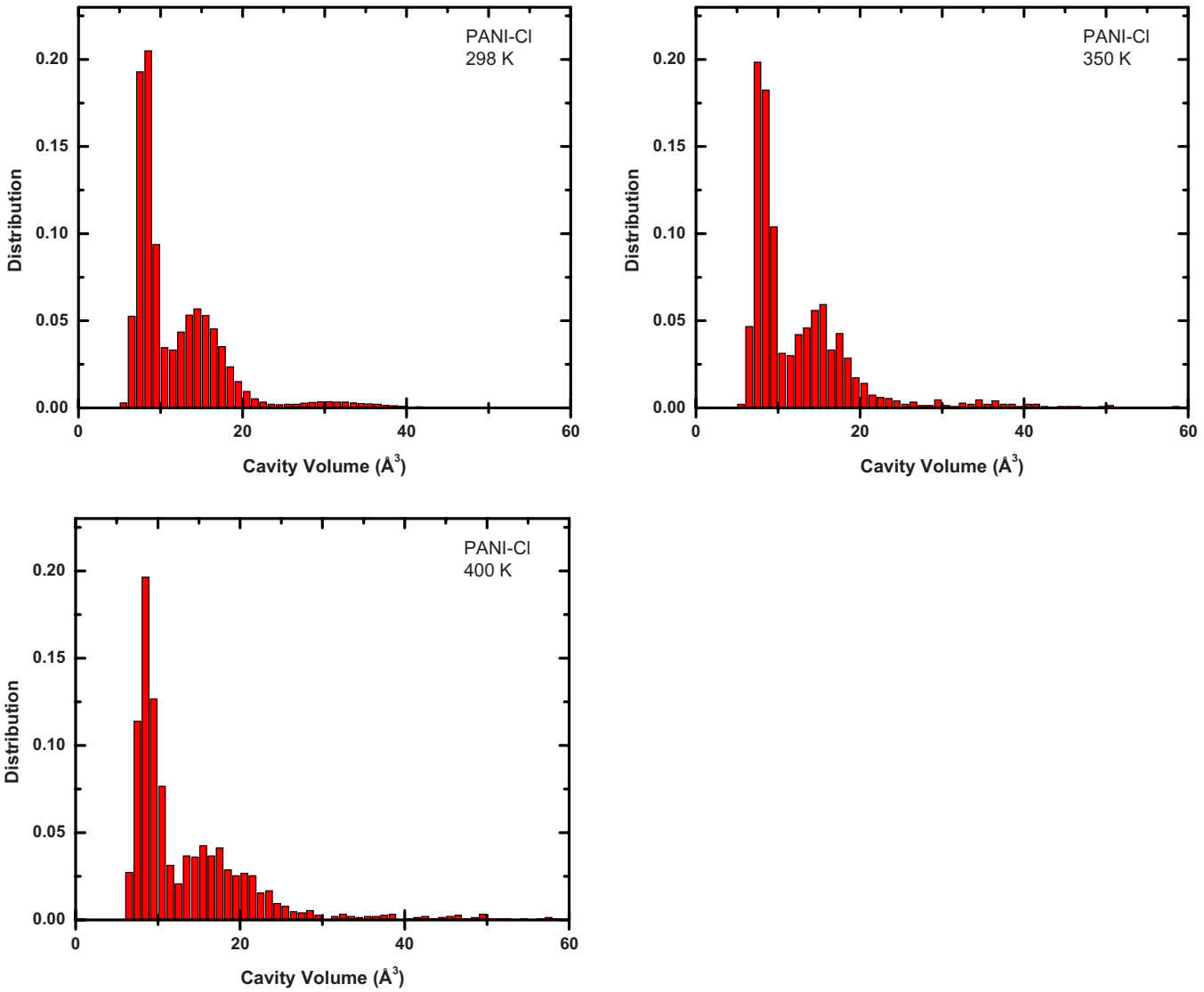

FIG. 6. (Color online) Computed cavity volume distribution of the PANI-Cl polymer and its dependence on temperature.

Another way of understanding how Cl, Br, and water molecules interact with each other and with the polymer is through computing the various pair-correlation functions $g(r)$. We computed such functions for Cl-N, Cl-H_2O, and similar pairs involving Br, as well as N-H_2O and H_2O-H_2O pairs in both the PANI-Cl and the PANI-Br. Figure 9 presents the results for the PANI-Cl at 350 K. As is well known, a peak in $g(r)$ corresponds to the distance between two atoms. Since the pair-correlation functions that we compute are for the pairs that involve nonbonded atoms and molecules and those in the PANI, the *sum* of the van der Waals radii yields a good indicator of how the various atoms or molecules are located with respect to one another. In Fig. 9 the arrows indicate the sum of the van der Waals radii of the atoms or molecules in the pair-correlation functions. Comparing $g(r)$ for the Cl-N and N-H_2O pairs with those for the other two pairs indicates that the nitrogen atom on the polymer chain is more accessible to H_2O. This is indicated by the peak positions at the shorter distances. Compared with nitrogen, the anion Cl^- is less accessible to H_2O. This is indicated by the weak peaks in the pair-distribution functions. Such arrangements of the atoms and molecules have been shown to be responsible for water adsorption in conducting polymers [7,43]. The two sharp peaks in the water-water pair-correlation function indicate self-aggregation of H_2O molecules.

Note that, as the inset in the water-water pair-correlation function (the lower right figure in Fig. 9) indicates, there is a pronounced peak around 3.5 Å but, due to scale of $g(r)$ on the vertical axis of the main figure, the peak is not very clear. The reason is that both the O-H and H-H bonds are included in the computed $g(r)$. These are indicated by two peaks in $g(r)$, with the first peak being at 1 Å that corresponds to the O-H bond, while the second peak is at 1.5 Å that represents the H-H distance. The peak in the inset of the figure (not pronounced in the main curve) at 3.5 Å is due to the O-O distance. This was confirmed by separately computing the pair-correlation function for the O-O bonds. The resulting $g(r)$ had a peak at about 3.5 Å.

Qualitatively similar behavior is also obtained with the PANI-Br, for which Fig. 10 presents the results at 350 K. Raising the temperature does not make a qualitative differ-

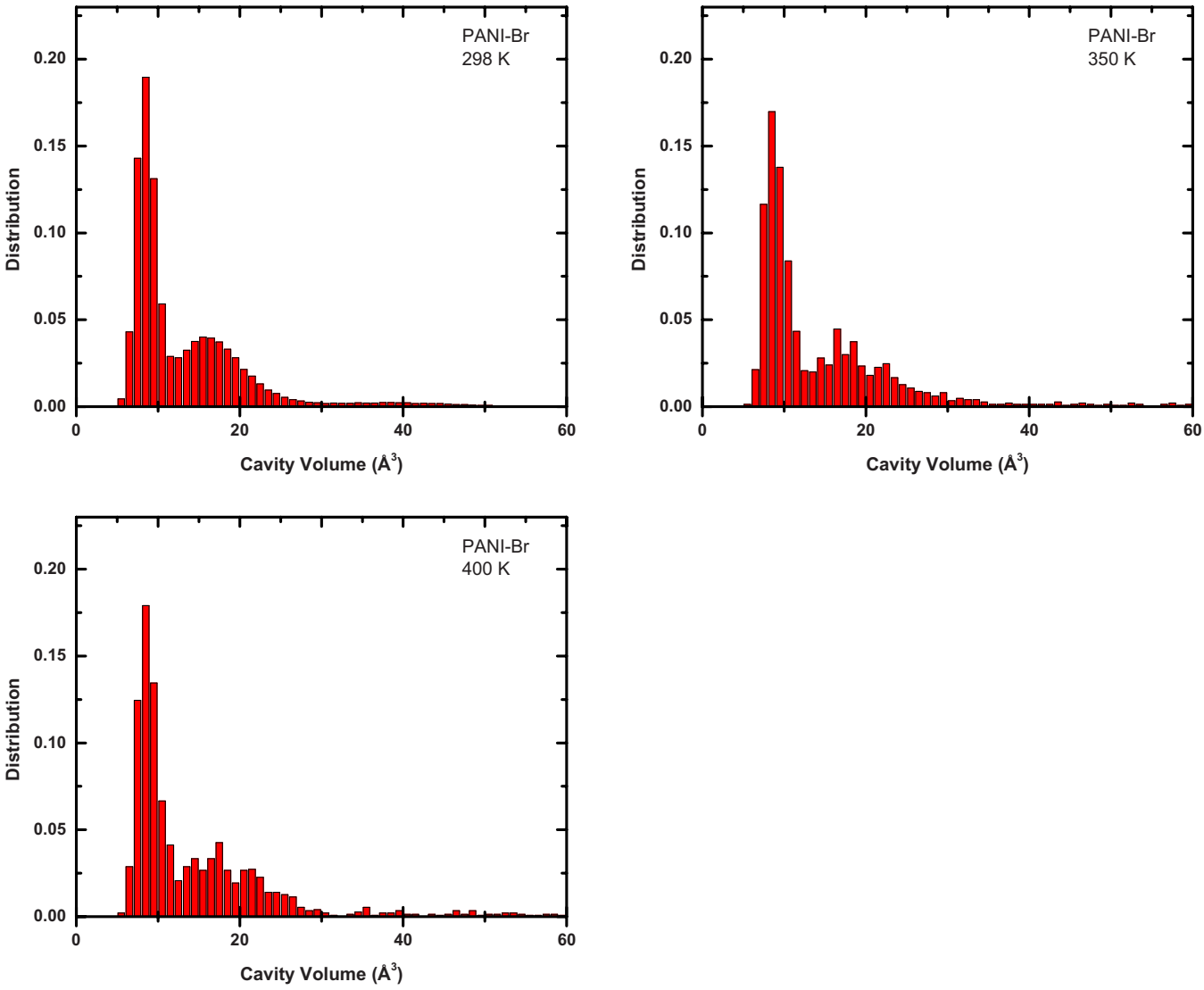

FIG. 7. (Color online) Same as in Fig. 6, but for the PANI-Br polymer.

ence in the computed pair-correlation functions, at least so long as the increase in T is moderate. Figure 11 presents the results for the PANI-Cl at 400 K. While the positions of the peaks have changed somewhat, the qualitative patterns of the various pair-correlation functions have not.

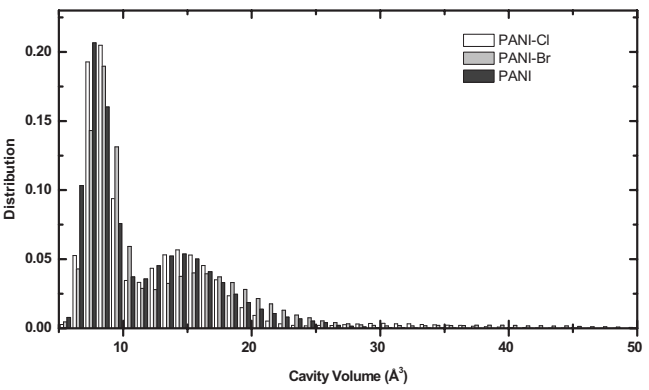

FIG. 8. Comparison of the cavity distributions of the doped PANI with that of the undoped polymer at 298 K.

B. Sorption isotherms

The cavity distributions, as well as the various pair distribution functions, provide a way of characterizing the differences between the two doped polymers and the interactions between the guest molecules (Cl, Br, and H_2O) and the polymers and, therefore, the rate of diffusion in them. The differences between the sorption properties of the two conducting polymers may be quantified by the fluctuations in the excess chemical potentials μ_e of the system, when the guest molecules are inserted in the polymers. We show in Fig. 12 the time dependence of μ_e when H_2O is added to the two doped polymers, using the particle-insertion method. Generally speaking, μ_e fluctuates more widely with the time in the PANI-Cl than in the PANI-Br. The reason is again tied to the cavity distribution: the PANI-Cl has a larger number of small cavities than the PANI-Br. In fact, if we plot the time evolution of the cavity size distributions, we find similar fluctuation patterns.

The computed isotherms, based on the particle-insertion method, for adsorption of water in the PANI-Cl at several

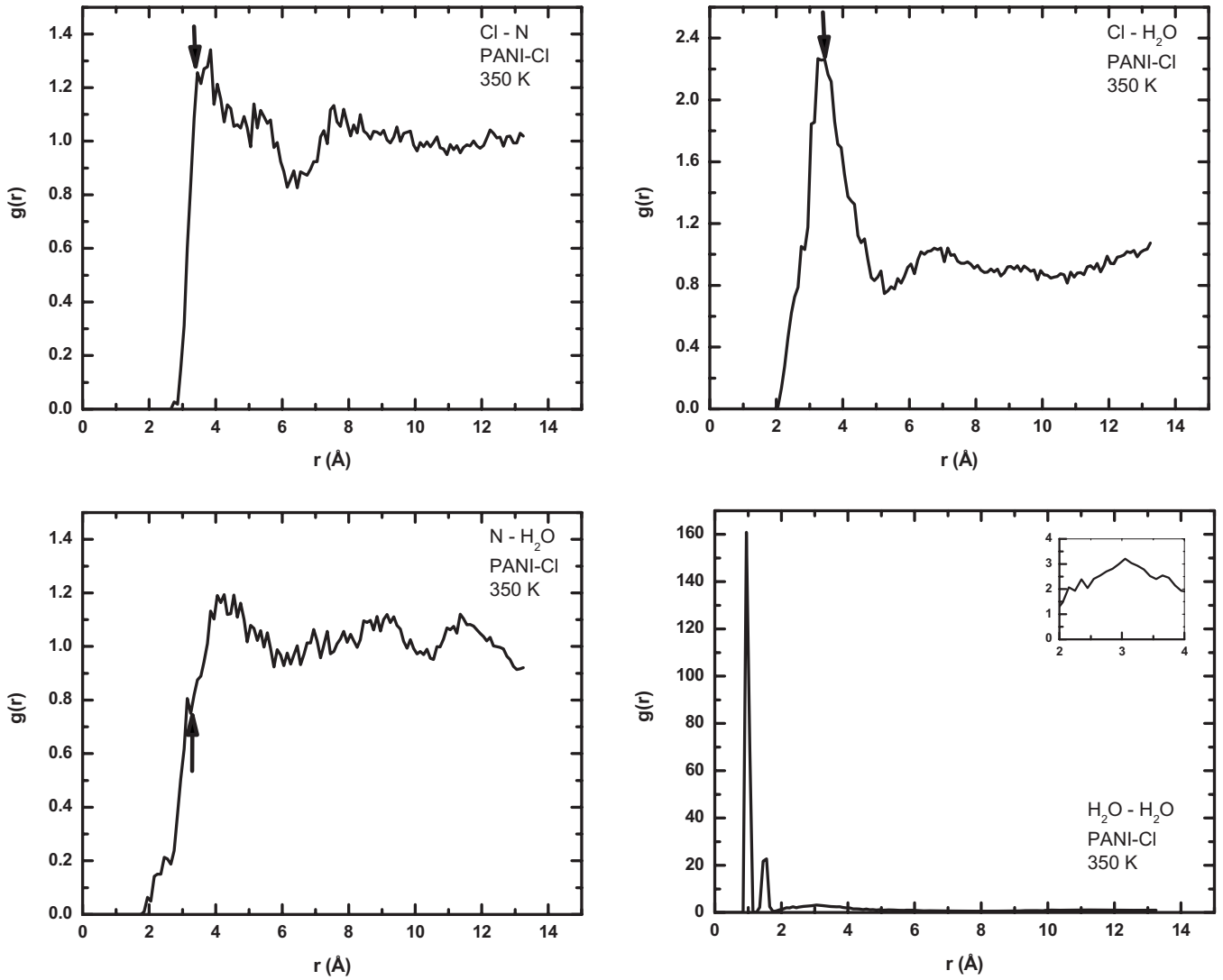

FIG. 9. Pair-distribution functions $g(r)$ for various atoms and molecules in the PANI-Cl at 350 K. The inset for the H_2O-H_2O case shows the peak in the pair-correlation function that corresponds to the O-O distance.

temperatures are presented in Fig. 13. Also shown is the measured isotherm at 298 K, reported previously by us [3,4]. q, which represents mg of water adsorbed per gram of the sample shown on the vertical axis of the figure, was calculated by

$$q = \frac{18015.2 n_w}{182.22 + M_a}. \tag{12}$$

Here, n_w is the number of water molecules per repeat unit, M_a is the molecular mass of the anion (35.45 g/mol for Cl^- and 79.90 g/mol for Br^-), and the numbers 18015.2 (with units mg/mol) and 182.22 (with units g/mol) represent, respectively, the molecular masses of H_2O and of the PANI's repeating unit, where each bracket in Fig. 1(b) is considered as a repeat unit. The agreement between the measured and computed isotherms at 298 K is excellent.

As the temperature increases, the adsorbed amount of H_2O decreases, which is expected. But, more importantly, the qualitative features of the sorption isotherms also change with increasing temperature. While at room temperature (298 K), the adsorbed amount rises sharply with small increases in the pressure, indicating a phase transition, the increase is much slower at high temperatures.

As mentioned above, the adsorption isotherms were also computed using the GCMC method. One goal of the GCMC simulations was to see whether it reproduces the results obtained by the particle-insertion method. The simulations were carried out at the highest and lowest temperatures, namely, 298 and 375 K. Both the PC and COMPASS force fields were utilized. We found that (i) the GCMC-computed isotherms at 298 K, using both force fields, predict, by 2–3 orders of magnitude, lower amounts of adsorbed water in the polymers than what we obtain with the particle-insertion method and (ii) the isotherms at 375 K, computed by both the particle-insertion and GCMC methods, using the PC force field, agree very well.

Figure 14 presents the isotherms for the PANI-Cl at 298 K, computed by the GCMC and both force fields (the results are identical). While, for example, at a pressure of 1 kPa the

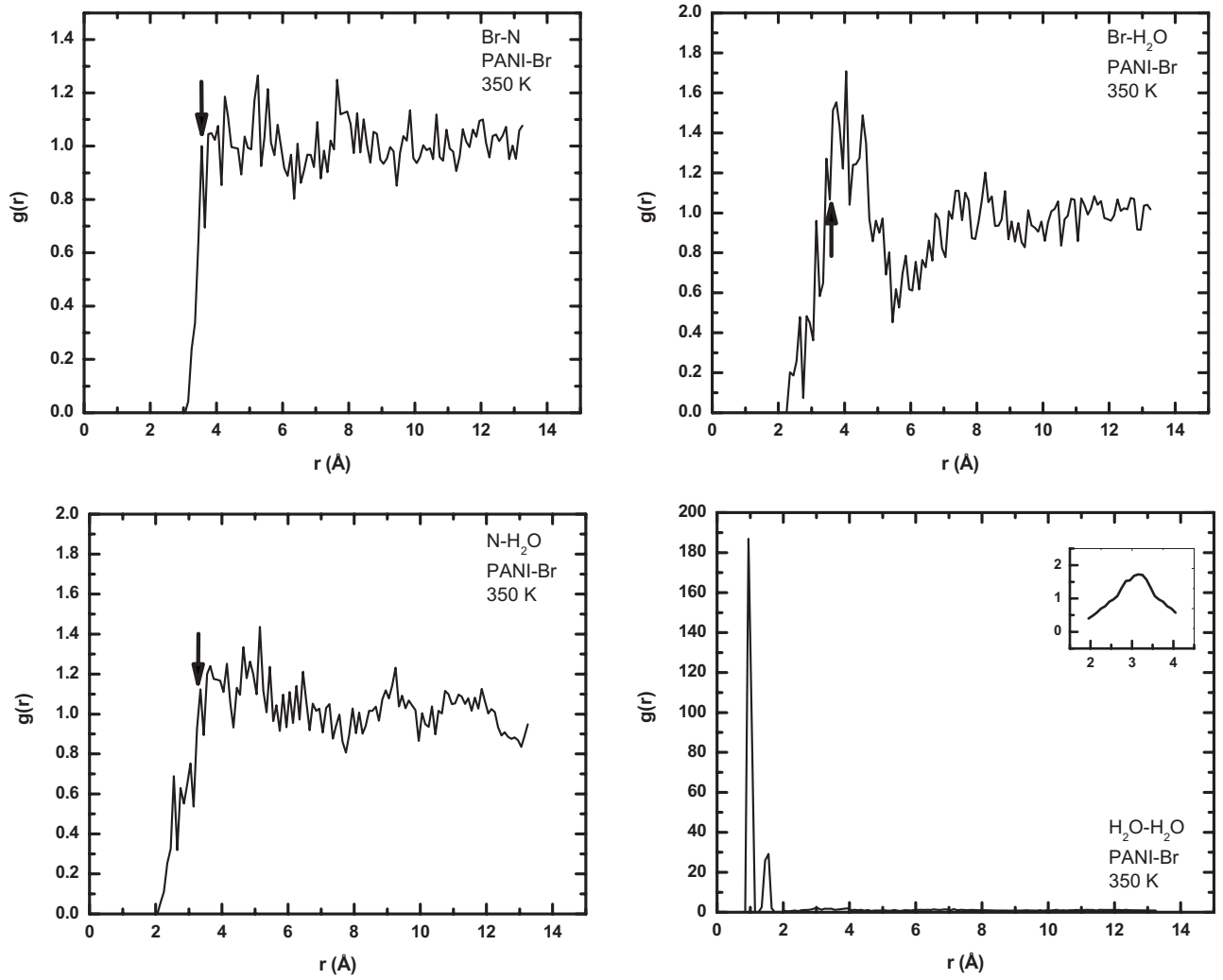

FIG. 10. Same as in Fig. 9, but for PANI-Br.

amount of adsorbed water obtained by the particle-insertion method is about 42 mg of H_2O/g of the sample—which agrees with the experimental measurement—the corresponding number obtained with the GCMC method is about 0.025 mg of H_2O/g of the sample, which is about 1700 smaller.

At first, the difference may seem surprising, since the particle-insertion method and the GCMC should, in principle, yield the same results, at least for certain gases. However, inspection of Fig. 13 reveals the reason for the difference. As both the experiments and the particle-insertion computations at 298 K indicate, there is a sharp, presumably first-order, phase transition at this temperature. It is known [36,44] that the GCMC method is sensitive to the initial state of the system. Thus, if one uses the GCMC method for computing the sorption isotherm in a system near the phase transition, one may start in the "wrong" phase by demanding the system to be at the wrong chemical potential. In that case, it would take an inordinate amount of computation time to get out of that phase and move to the "right" phase. On the other hand, in the particle-insertion method one does not force the system to be at a given chemical potential. Instead, one can choose the right phase by inserting the correct number of the adsorbates and compute the corresponding chemical potential.

This picture is confirmed by the computations at 375 K. Figure 13 indicates no phase transition at this temperature. Thus, we may expect the two methods to yield essentially the same isotherms. This is, indeed, the case. Figure 15 compares the isotherms computed by the particle-insertion and GCMC methods at 375 K, using the PC force field. The two methods yield essentially the same isotherms. Thus, aside from the cases in which there is possibly a phase transition, the GCMC and particle-insertion methods should yield the same results, since they both are based on the insertion of the guest molecules in a stiff polymeric matrix.

It would be most interesting to use another method in which, rather than inserting the guest molecules, they are "grown in." One possible approach is the fast-growth thermodynamic integration method [45], which is based on a theorem by Jarzynski [46]. The theorem relates the work W_{AB} done on system, as a result of going from state A to state B, to a free-energy change, irrespective of the reversibility of the sampling. It is shown [46] that the exponentially averaged work of repeated sampling of the path from A to B is equal to the free-energy difference ΔE_{AB} between A and B,

$$\Delta E_{AB} = -k_B T \ln\langle \exp(-W_{AB}/k_B T)\rangle_A, \qquad (13)$$

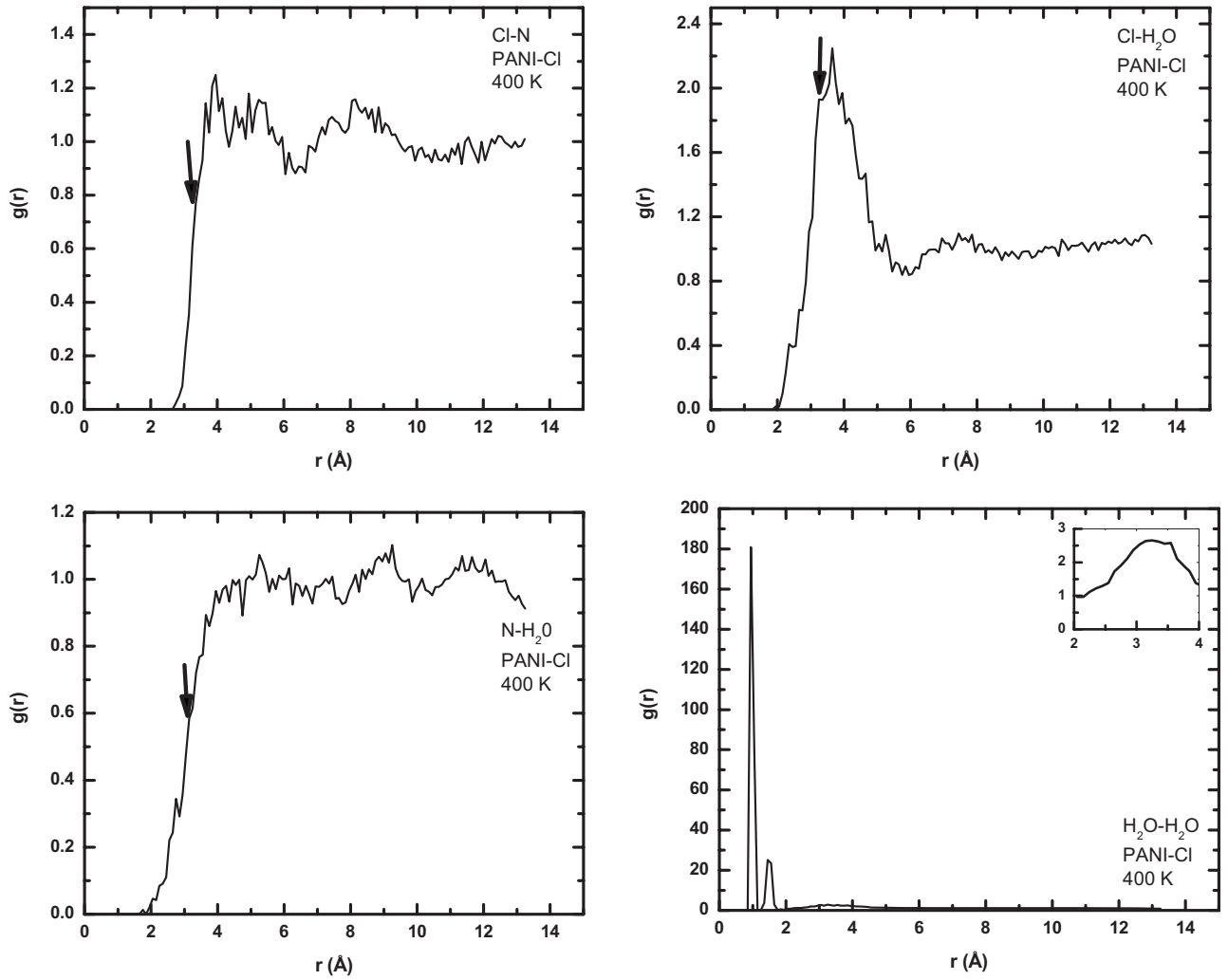

FIG. 11. Same as in Fig. 9, but at 400 K.

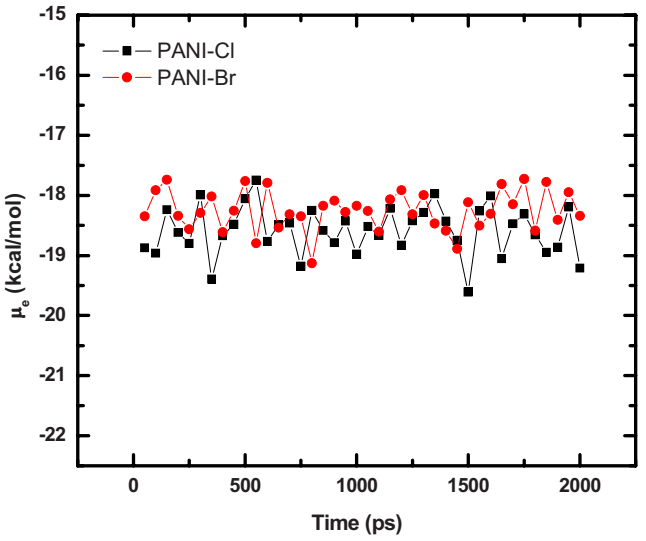

FIG. 12. (Color online) Fluctuations in time of the computed excess chemical potential μ_e of the PANI-Cl+water and PANI-Br +water systems at 350 K.

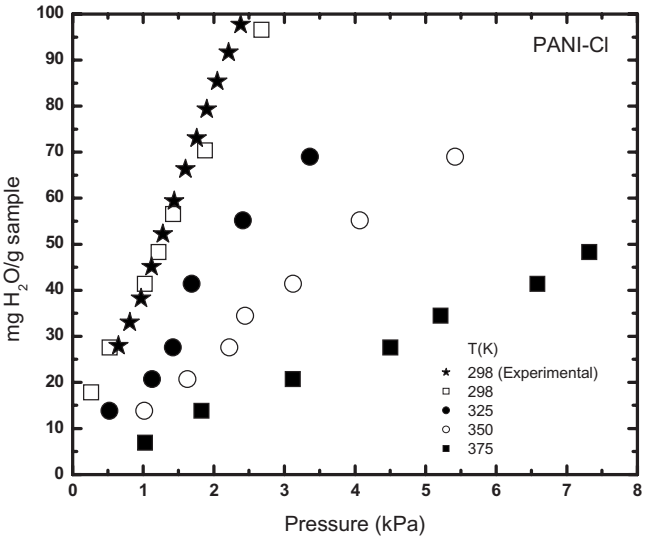

FIG. 13. Computed sorption isotherms of water in the PANI-Cl at various temperatures. The experimental data at 298 K are from Refs. [3,4].

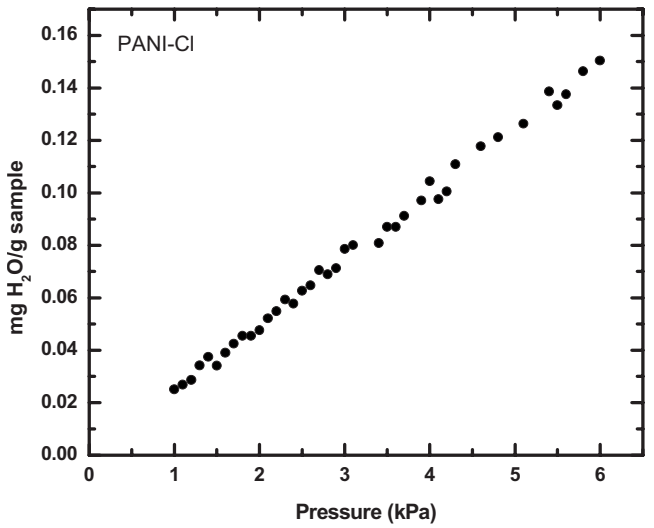

FIG. 14. Sorption isotherm of water in the PANI-Cl at 298 K, using the GCMC method and the PC force field.

where $\langle \cdot \rangle$ denotes averaging over a canonical ensemble of the initial state A. This theorem has led to a highly efficient method for computing the excess chemical potentials and, hence, determining the sorption isotherms.

Qualitatively similar patterns were also obtained for the adsorption of water vapor in the PANI-Br. The results are presented in Fig. 16, using the particle-insertion method. At the same time, although, there is a significant difference between the sorption isotherms of water in the two doped polymers: at any given temperature and pressure, the PANI-Cl adsorbs more water vapor than the PANI-Br, with the difference being 20% or more. This is directly tied with the cavity distributions of the two materials described above, and the larger fluctuations of the excess chemical potentials in the PANI-Cl, which has a larger number of smaller cavities. Such differences also indicate the significance of the doping agent for water adsorption. The qualitative trends in the isotherms are also consistent with the reported experimental data for the PANI doped with phosphoric acid at various temperatures [4], and the fundamental thermodynamic effects, as described there [4].

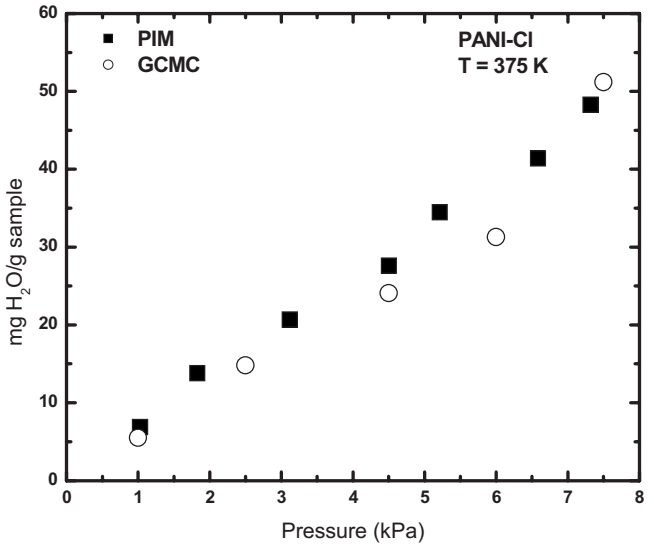

FIG. 15. Comparison of the sorption isotherms of water in the PANI-Cl at 375 K, computed using the PC force field, and the particle-insertion and GCMC methods.

TABLE V. Experimental and computed values of Henry's constant K (in K mg/g kPa), for water sorption isotherms in PANI-Cl and PANI-Br polymers.

T (K)	PANI-Cl		PANI-Br	
	Computed	Experiment	Computed	Experiment
298	32.51	40.98	28.83	29.50
325	20.88		19.89	
350	12.87		11.17	
375	6.30		5.66	

The experimental sorption data at 298 K were previously fitted [3,4] to a linear isotherm based on Henry's law, in order to describe water sorption in the doped polymeric materials. The model is given by

$$q = KP, \tag{14}$$

with K being the Henry's law constant and P being the pressure. Thus, we also fitted the computed isotherms to Eq. (11). The estimated values of Henry's constant K, so obtained, are listed in Table V. Given the agreement between the estimates of K at 298 K, obtained by using the experimental data and the sorption isotherm computed by the particle-insertion method, we are reasonably confident that estimates of K at other temperatures are also accurate.

C. Self-diffusion coefficients

The time dependence of the MSDs of the water molecules in the PANI-Cl and PANI-Br at several temperatures are displayed in Figs. 17 and 18, respectively. Both figures indicate

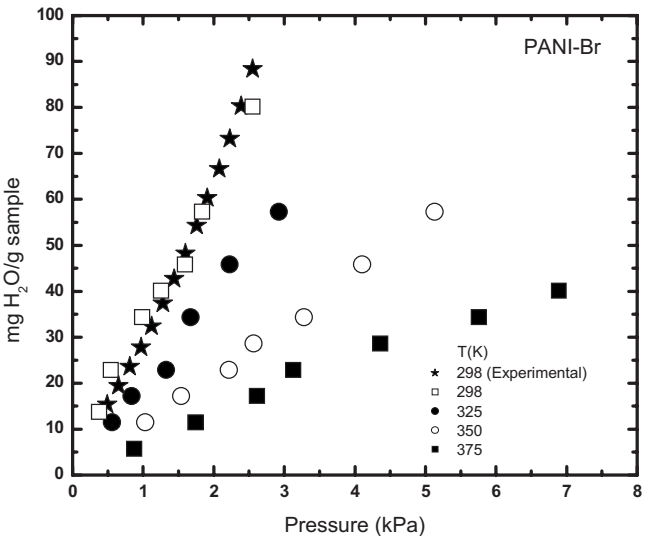

FIG. 16. Same as in Fig. 13, but for water in the PANI-Br.

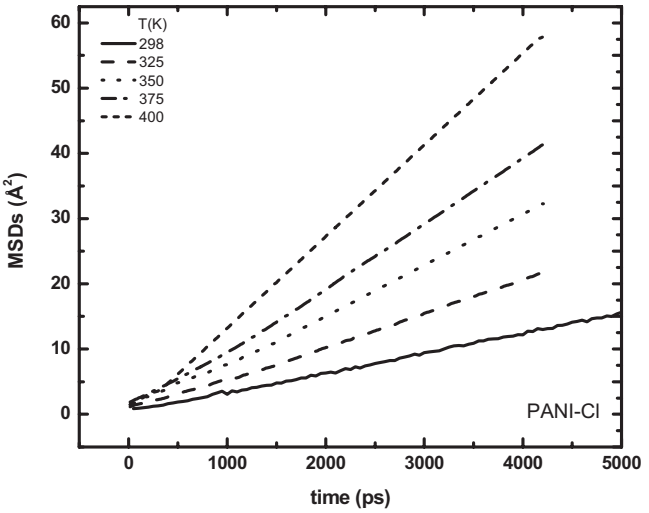

FIG. 17. Time dependence of the mean-square displacement (MSD) of water in the PANI-Cl at various temperatures.

that the magnitudes of the MSDs increase with increasing temperature. This is consistent with the fact that as T increases the density of the material decreases, hence resulting in more free volume for the H_2O molecules to move around (see the cavity volume distributions shown in Figs. 6 and 7). At the same time, higher temperatures results in higher kinetic energy for the water molecules. The two effects, when combined, result in higher MSDs for the water molecules at higher temperatures.

In order to be able to estimate the self-diffusivity of water vapor in the doped materials based on their MSDs, one must have diffusive transport in which the MSDs are a linear function of the time. For example, at 298 K the linear regime is reached after about 3.5 ns, but at higher temperatures the linear regime is reached over shorter periods of time. Examples are presented in Fig. 19, for both the PANI-Cl and the PANI-Br at 325 and 400 K. Transport of the water molecules in the PANI-Cl, for example, takes about 3 and 2.5 ns, in order to reach the diffusive regime at 325 and 400 K, respectively.

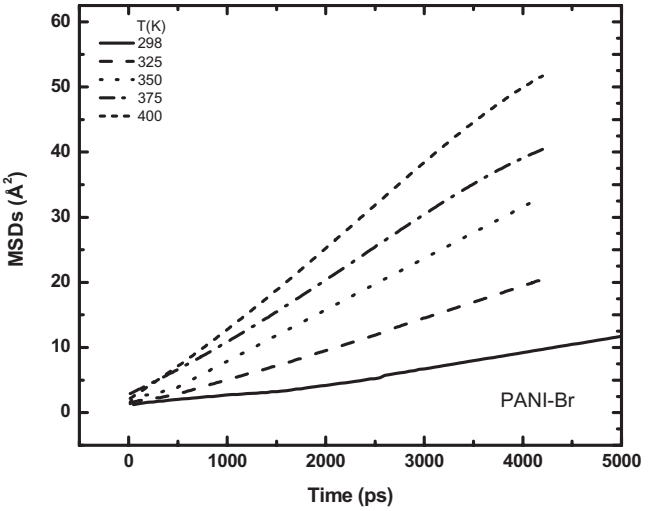

FIG. 18. Same as Fig. 17, but for water in the PANI-Br.

TABLE VI. Experimental and computed values of the self-diffusivity D ($\times 10^{12}$ m^2/s) of water vapor in PANI-Cl and PANI-Br polymers.

T (K)	PANI-Cl		PANI-Br	
	Computed	Experiment	Computed	Experiment
298	5.10	0.314	4.16	0.243
325	8.33		7.78	
350	12.40		12.90	
375	16.30		15.68	
400	23.20		20.60	

The computed diffusivities are listed in Table VI. The only experimental data for the self-diffusivity of water vapor in doped PANI that we are aware of are our own measurements [3,4] for dense *fibrous* doped PANI at 298 K. They are $D \simeq 3.14 \times 10^{-9}$ cm^2/s for the PANI-Cl and $D \simeq 2.43 \times 10^{-9}$ cm^2/s for the PANI-Br. We should, however, be cautious in making a direct comparison between the computed diffusivities and the data. It is well known that [47] that the distribution of the free volumes of a polymer is the most

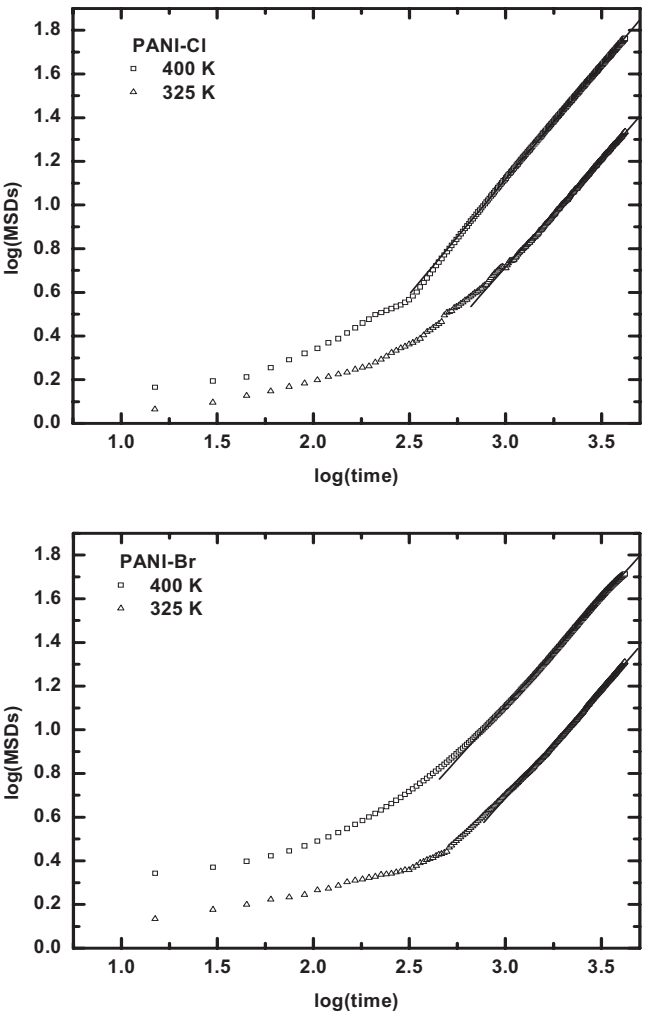

FIG. 19. Logarithmic plot of the MSDs vs time.

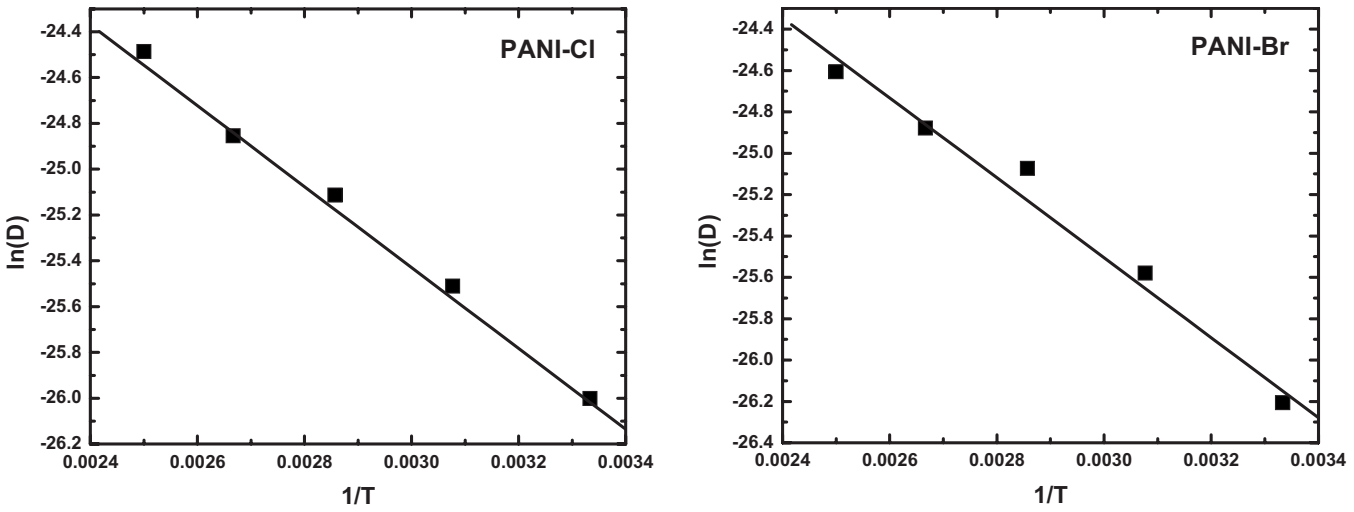

FIG. 20. ln(D) vs inverse of the temperature T. The straight lines represent the fits of the computed diffusivities to Eq. (16).

important factor in determining the self-diffusivity of a small gas molecule in the polymer. We expect the free-volume distribution of fibrous doped PANI not to be identical with those of the nonfibrous doped polymers. In addition, at least in the case of the PANI-Cl, the density of the simulated polymer ($1.2\ \mathrm{g/cm^3}$) is smaller than the experimental value ($1.3\ \mathrm{g/cm^3}$), implying a more open structure and, therefore, a larger self-diffusivity for the simulated polymer, which is consistent with the result.

We do point out, however, that, as the comparison of the computed and measured densities and the sorption isotherms at 298 K indicate, the structures of the doped polymers that were generated by the atomistic simulations are accurate representation of the actual polymers. Moreover, the computed ratio of the diffusivities, $D_{\mathrm{PANI\text{-}Cl}}/D_{\mathrm{PANI\text{-}Br}} \simeq 1.22$, which should be much less sensitive to the polymer structure, is close to experimental value of 1.29 for the fibrous PANIs.

D. Activation energies

There is yet another way of testing the accuracy of the estimated diffusivities. Assuming an activated diffusion process, and fitting the computed diffusivities at various temperatures to the Arrhenius equation,

$$D = D_0 \exp(-E/RT), \tag{15}$$

or,

$$\ln D = \ln D_0 - E/RT, \tag{16}$$

we may estimate the activation energy E from the slope of the straight line indicated by Eq. (16). Figure 20 presents plots of ln(D) versus $1/T$, along with the fitted straight lines. From the slopes of the straight lines, the estimated activation energies are $E \simeq 14.76$ kJ/mol for the PANI-Cl+water system and $E \simeq 15.79$ kJ/mol for the PANI-Br+water system. These estimates are within 25% of the value reported in the literature [43], which is about 21.00 kJ/mol. The relative accuracy of the estimated E provides further evidence that the computed diffusivities are realistic and accurate. But, due to the exponential dependence of D on the temperature, one must be cautious about drawing definitive conclusion from the agreement.

V. SUMMARY

Using energy minimization, molecular dynamics simulations, and the polymer-consistent and COMPASS force fields, atomistic models of amorphous polyaniline, doped by Cl and Br, were generated. The computed density of the doped polymers and sorption isotherms of water in the doped polymers at 298 K are in good agreement with the experimental data. Although we have no experimental data to directly compare with the computed self-diffusivities of water vapor in PANI-Cl and PANI-Br, the activation energies that we estimate based on the computed temperature dependence of the diffusivities are also in reasonable agreement with the experimental data.

Altogether, the results indicate the accuracy and validity of the atomistic model of the doped PANI that we studied. Therefore, we can now use the model as a tool for investigating the possibility of doping PANI with other halogen acids in order to explore the possibility of increasing the amount of water harvesting from the air by the PANI, as well as to study the conducting polymer's other potential applications.

ACKNOWLEDGMENTS

Partial support of this work by DARPA is gratefully acknowledged. We would like to thank Dr. Katherine S. Shing for useful discussions regarding the GCMC and particle-insertion methods. We are grateful to Dr. Maria Entrialgo-Castano for carrying out the sorption computations with the COMPASS force field.

[1] Climate Change 2007, Synthesis Report, http://www.ippc.ch/pdf/assessment-report/ar4/syr/ar4_sys_cover.pdf
[2] Water Extraction Technologies, Water From Air, http://www.sciperio.com/watertech/water-from-air.asp
[3] M. M. Ostwal, J. J. Pellegrino, I. D. Norris, T. T. Tsotsis, M. Sahimi, and B. R. Mattes, Ind. Eng. Chem. Res. **44**, 7860 (2005).
[4] M. M. Ostwal, B. Qi, J. J. Pellegrino, A. G. Fadeev, I. D. Norris, T. T. Tsotsis, M. Sahimi, and B. R. Mattes, Ind. Eng. Chem. Res. **45**, 6021 (2006).
[5] J. J. Pellegrino, in *Advanced Membrane Technology*, Vol. 984 of Annals New York Academy of Sciences, edited by N. N. Li, E. Drioli, W. S. W. Ho, and G. G. Lipscomb (New York Academy of Science, New York, 2003), p. 289.
[6] M. Nechtschein, C. Santier, J. P. Travers, J. Chroboczek, A. Alix, and M. Ripert, Synth. Met. **18**, 311 (1987).
[7] B. Z. Lubentsov, O. N. Timofeeva, and M. L. Khidekel, Synth. Met. **45**, 235 (1991).
[8] T. Taka, Synth. Met. **57**, 5014 (1993).
[9] B. Z. Lubentsov, O. N. Timofeeva, S. Saratovskikh, V. Krinichnyi, A. Pelekh, V. Dmitrenko, and M. L. Khidekel, Synth. Met. **47**, 187 (1992).
[10] A. Alix, V. Lemoine, M. Nechtschein, J. P. Travers, and C. Menardo, Synth. Met. **29**, 457 (1989).
[11] J. P. Travers, Synth. Met. **55**, 731 (1993).
[12] T. A. Skotheim, R. L. Elsenbaumer, and J. R. Reynolds, *Handbook of Conducting Polymers* (Marcel Dekker, New York, 1998).
[13] M. F. Hundley, P. N. Adams, and B. R. Mattes, Synth. Met. **129**, 291 (2002).
[14] C. R. A. Catlow and G. E. Mills, Electrochim. Acta **40**, 2057 (1995).
[15] D. Alperstein, M. Narkis, M. Zilberman, and A. Siegmann, Polym. Adv. Technol. **9**, 563 (1998).
[16] A. M. Almeida, M. M. D. Ramos, and R. M. Ribeiro, Macromol. Symp. **181**, 479 (2002).
[17] E. Spohr, P. Commer, and A. A. Kornychev, J. Phys. Chem. B **106**, 10560 (2002).
[18] O. Borodin and G. D. Smith, Macromolecules **33**, 2273 (2000).
[19] D. N. Theodorou and U. W. Suter, Macromolecules **18**, 1467 (1985).
[20] E. Tocci, D. Hofmann, D. Paul, N. Russo, and E. Drioli, Polymer **42**, 521 (2001); M. M. Ostwal, T. T. Tsotsis, and M. Sahimi, J. Chem. Phys. **126**, 124903 (2007).
[21] A. R. Mehrabi and M. Sahimi, Phys. Rev. Lett. **82**, 735 (1999).
[22] (a) N. Kim, A. Harale, T. T. Tsotsis, and M. Sahimi, J. Chem. Phys. **127**, 224701 (2007); (b) A. R. Mehrabi and M. Sahimi, *ibid.* **128**, 234503 (2008).
[23] D. Wolf, P. Keblinski, S. R. Phillpot, and J. Eggebrecht, J. Chem. Phys. **110**, 8254 (1999).
[24] H. Sun, J. Phys. Chem. B **102**, 7338 (1998).
[25] Since we did not have access to the licensed package of CERIUS[2] simulator, Dr. Maria Entrialgo-Castano of Accelyrs (United Kingdom) kindly carried out the calculations for us.
[26] M. Sahimi, *Heterogeneous Materials II: Nonlinear and Breakdown Properties and Atomistic Modeling* (Springer, New York, 2003), Chap. 8.
[27] M. Sniechowski, D. Djurado, B. Dufour, P. Rannou, A. Pron, and W. Luzny, Synth. Met. **143**, 163 (2004); M. Sniechowski, D. Djurado, M. Bée, M. A. Gonzaqlez, M. R. Johnson, P. Rannou, B. Dufour, and W. Luzny, Chem. Phys. **317**, 289 (2005).
[28] W. L. Jorgensen, J. Chandrasekhar, J. D. Madura, R. W. Impey, and M. L. Klein, J. Chem. Phys. **79**, 926 (1983).
[29] H. J. C. Berendsen, J. R. Grigera, and T. P. Straatsma, J. Phys. Chem. **91**, 6269 (1987).
[30] A. Striolo, K. E. Gubbins, M. S. Gruszkiewicz, D. R. Cole, J. M. Simonson, A. A. Chialvo, P. T. Cummings, T. D. Burchell, and K. L. More, Langmuir **21**, 9457 (2005); A. Striolo, A. A. Chialvo, K. E. Gubbins, and P. T. Cummings, J. Chem. Phys. **122**, 234712 (2005).
[31] E. Stöckelmann and R. Hentschke, Langmuir **15**, 5141 (1999).
[32] E. A. Müller, F. R. Hung, and K. E. Gubbins, Langmuir **16**, 5418 (2000).
[33] J. Z. Yang, Q. L. Liu, and H. T. Wang, J. Membr. Sci. **291**, 1 (2007).
[34] A. Rahaman, V. H. Grassian, and C. J. Margulis, J. Phys. Chem. C **112**, 2109 (2008).
[35] J. W. Caldwell and P. A. Kollman, J. Phys. Chem. **99**, 6208 (1995).
[36] M. Sahimi and T. T. Tsotsis, in *Handbook of Theoretical and Computational Nanotechnology*, edited by M. Rieth and W. Schommers (American Scientific, New York, 2006), Chap. 10.
[37] H. C. Andersen, J. Chem. Phys. **72**, 2384 (1980).
[38] S. Nosé, J. Chem. Phys. **81**, 511 (1984); W. G. Hoover, Phys. Rev. A **31**, 1695 (1985).
[39] V. G. Mavrantzas, T. D. Boone, E. Zervopoulou, and D. N. Theodorou, Macromolecules **32**, 5072 (1999); R. Auhl, R. Everaers, G. S. Grest, K. Kremer, and S. J. Plimpton, J. Chem. Phys. **119**, 12718 (2003).
[40] B. Widom, J. Chem. Phys. **39**, 2808 (1963); J. Phys. Chem. **86**, 869 (1982); G. L. Deitrick, L. E. Scriven, and H. T. Davis, J. Chem. Phys. **90**, 2370 (1989).
[41] J. K. Johnson, J. A. Zollweg, and K. E. Gubbins, Mol. Phys. **78**, 591 (1993).
[42] M. Tanemura, T. Ogawa, and N. Ogita, J. Comput. Phys. **51**, 191 (1983).
[43] E. S. Matveeva, R. D. Calleja, and V. P. Parkhutik, Synth. Met. **72**, 105 (1995).
[44] D. Frenkel and B. Smit, *Understanding Molecular Simulations* (Academic, San Diego, 1996).
[45] D. A. Hendrix and C. Jarzynski, J. Chem. Phys. **114**, 5974 (2001); G. Hummer, *ibid.* **114**, 7330 (2001); B. Hess, C. Peter, T. Ozal, and N. F. A. van der Vegt, Macromolecules **41**, 2283 (2008).
[46] C. Jarzynski, Phys. Rev. Lett. **78**, 2690 (1997); see also, G. Hummer and A. Szabo, Proc. Natl. Acad. Sci. U.S.A. **98**, 3658 (2001).
[47] M. Meunier, J. Chem. Phys. **123**, 134906 (2005).